

High energy muons in extensive air showers

C. Gámez*, M. Gutiérrez, J.S. Martínez, M. Masip

*CAFPE and Departamento de Física Teórica y del Cosmos
Universidad de Granada, E-18071 Granada, Spain*

car,mgg,jsilverio,masip@ugr.es

Abstract

The production of very high energy muons inside an extensive air shower is observable at ν telescopes and sensitive to the composition of the primary cosmic ray. Here we discuss five different sources of these muons: pion and kaon decays; charmed hadron decays; rare decays of unflavored mesons; photon conversion into a muon pair; and photon conversion into a J/ψ vector meson decaying into muons. We solve the cascade equations for a $10^{10.5}$ GeV proton primary and find that unflavored mesons and gamma conversions are the two main sources of $E \geq 10^{8.5}$ GeV muons, while charm decays dominate at $10^{5.5} \text{ GeV} < E < 10^{8.5} \text{ GeV}$. In inclined events one of these muons may deposit a large fraction of its energy near the surface, implying fluctuations in the longitudinal profile of the shower and in the muon to electron count at the ground level. In particular, we show that 1 out of 6 proton showers of $10^{10.5}$ GeV include an $E > 10^6$ GeV deposition within 500 g/cm^2 , while only in 1 out of 330 showers it is above 10^7 GeV. We also show that the production of high energy muons is very different in proton, iron or photon showers (*e.g.*, conversions $\gamma \rightarrow \mu^+ \mu^-$ are the main source of $E \geq 10^4$ GeV muons in photon showers). Finally, we use Monte Carlo simulations to discuss the validity of our results.

*Now at CIEMAT, Avenida Complutense 22, E-28040 Madrid, Spain

1 Introduction

Extensive air showers (EASs) initiated by ultrahigh energy cosmic rays (CRs) include millions of collisions and decays of secondary particles. These showers can be observed with fluorescence detectors, able to measure energy depositions as the shower develops along the atmosphere, and/or surface detectors, which register energy depositions of the particles reaching the ground. Despite the large number of processes involved in an individual EAS, its dynamics can be understood within the following simplified scheme [1].

Let us take a proton primary facing a relatively large slant depth (*e.g.*, $X \approx 2000 \text{ g/cm}^2$ from a zenith angle $\theta_z \approx 60^\circ$). The first interaction will take place high in the atmosphere, after the proton has crossed a hadronic interaction length ($\lambda_{\text{int}} \approx 41 \text{ g/cm}^2$ at $E = 10^{10} \text{ GeV}$). It will result into a leading baryon carrying around 25% of the initial energy plus dozens of light mesons (mostly pions) sharing the rest of the energy. The leading baryon will interact again deeper into the atmosphere, but after just four collisions 99% of its energy will already be transferred to pions. High energy charged pions, in turn, may collide giving more pions of lower energy or they may decay into leptons, $\pi^+ \rightarrow \mu^+ \nu_\mu$. Decays are only favoured at relatively low energies, below (with a strong dependence on the altitude) 50 GeV, so the production of very high energy muons and neutrinos is suppressed. In contrast, neutral pions of all energies decay almost instantly ($\pi^0 \rightarrow \gamma\gamma$) giving photons that feed the electromagnetic (EM) component of the EAS. Photons will convert into e^+e^- pairs after $9X_0/7 \approx 47 \text{ g/cm}^2$, whereas electrons will radiate half their energy after a similar depth, so the EM energy is transformed fast into a large number of lower-energy particles that define the shower maximum at $X_{\text{max}} \approx 800 \text{ g/cm}^2$. The precise position of X_{max} has fluctuations $\Delta X_{\text{max}} \approx 50 \text{ g/cm}^2$ that depend basically on the details in the first few collisions of the leading baryon. Notice also that most of the energy in the EAS will be processed through gammas and electrons instead of muons and neutrinos: although the three pion species are created at a similar rate, high-energy charged pions tend to collide giving both charged and neutral pions, whereas all the energy that goes into neutral pions becomes EM and has a small return to hadrons. In inclined events, after a depth around $2X_{\text{max}}$ most gammas and electrons have been absorbed by the atmosphere and the signal becomes dominated by muons, although it includes an EM *tail* created by muon radiative depositions and muon decays.

Within this simple picture, the value of X_{max} or the signal at the surface detectors depend critically on the inelasticity (fraction of energy lost by the leading hadron) and the multiplicity (number of secondary hadrons that share that energy) in nucleon and pion collisions in the air. Unfortunately, the study of these two observables at colliders is not easy, as it involves a very wide range of energies and a kinematical region (ultraforward) of difficult access.[†] The uncertainty that they introduce (for example, through the appearance of collective effects [3]) could possibly explain the apparent 50% excess in the number of muons at the ground level recently emphasized by the

[†]A forward spectrometer at the LHC appears indeed as a very promising possibility [2].

Pierre Auger Observatory [4]. Nevertheless, the picture provides a good description of the main features in an EAS. The different values of X_{\max} for proton or iron primaries, for example, are easily understood if one sees a nucleus shower as the superposition of A nucleon showers of energy E/A , each one with a smaller value of X_{\max} .

However, there are a few features in an EAS that are in principle observable and require a more elaborate scheme. The production of $E \geq 10^5$ GeV neutrinos is one of them: It is expected that at those energies pion and kaon decays become a less effective source of neutrinos than charmed hadron decays [5,6]. Another one are the muons of also very high energy. The weak decays of mesons produce both muons and neutrinos, but muons may also appear with no neutrinos in the EM decays of unflavored mesons or in the interactions of high energy photons with atmospheric nuclei [7,8]. These relatively rare processes are not always included in Monte Carlo simulations, in particular, some rare decays of unflavored mesons are absent in EPOS-LHC [9] and only the most recent version of SIBYLL [10] includes the production of charmed hadrons. Our first objective in this work is to review and compare the different production channels of high energy muons inside an EAS.

We find several phenomenological reasons why these most energetic muons may be interesting. First, they could be useful in composition studies. Obviously, an iron shower will never contain a muon carrying a fraction of energy larger than $1/A = 0.017$; but how frequent are muons with, for example, a 0.1% of the shower energy? It turns out that such muons are 10 times more likely in a proton than in an iron EAS. They will often appear in pairs, in the core of the shower, always accompanied by a bundle of lower energy muons. Their inclination when they cross a neutrino telescope and/or catastrophic energy losses there would reveal the minimum energy of these muons [11–13].

Another phenomenological reason of interest rarely explored in the literature (see for example [14]) is their possible effect on the longitudinal development of inclined EASs. It has been shown [15] that the ratio $r_{\mu e}$ of the muon to EM signals at the ground level (number of muons over total EM energy at the surface detectors) is strongly correlated with the position of the shower maximum, and that the correlation seems to be independent from the hadronic model used in the simulation. Since the fluctuations between two showers from identical primaries are basically caused by the initial hadronic processes, the great stability in the $r_{\mu e}-X_{\max}$ correlation (due only to collisions and decays *after* the shower maximum) is not surprising. In a search for possible heavy quark effects in EASs, the analysis with the code AIRES [16] in [15] finds that sometimes a very energetic muon created in D or B decays introduces anomalies in that ratio. Indeed, an $E > 10^6$ GeV deposition near the ground (when most of the shower energy has already been absorbed) in an inclined ($\theta_z \geq 60^\circ$) event could change substantially the signal at the surface detectors. The programmed upgrade at AUGER [17] may provide a more precise separation of the muon and EM signals, so it seems interesting an estimate of how frequent such muon energy depositions are and what their origin (in addition to heavy quark decay) may be. This is precisely our second objective in this work.

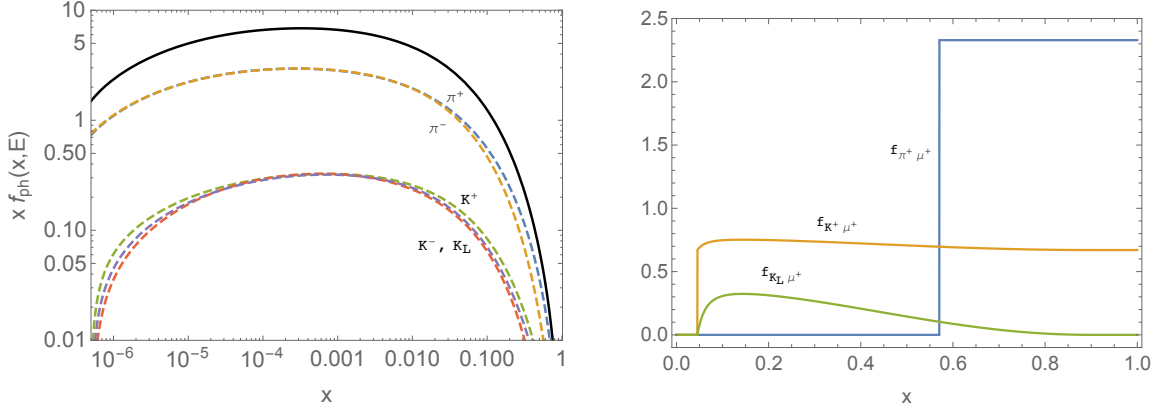


Figure 1: Pion and kaon yields in proton-air collisions at 10^6 GeV obtained with EPOS-LHC (left) and muon yields in pion and kaon decays (right).

The plan of this article is as follows. In the next section we review the different processes that may produce high energy muons inside an EAS. In section 3 we solve the cascade equations for the average $10^{10.5}$ GeV proton, iron or gamma shower and we deduce the spectrum of muons reaching the ground from large zenith inclinations. In section 4 we parametrize the three main radiative processes experienced by a muon in the air (bremsstrahlung, pair production and photonuclear collisions) and we estimate the probability for a large energy deposition near the surface. Finally, in section 5 we discuss the validity of our method by comparing with Monte Carlo simulations and we conclude in section 6.

2 Muon production channels

(i) *Conventional muons from pion and kaon decays.*

We have obtained a fit[‡] for the yields $f_{hh'}(x, E)$ of hadrons $h' = p, n, \bar{p}, \bar{n}, \pi^\pm, K^\pm, K_L$ produced in the collisions of nucleons, pions and kaons of energy E with an average air nucleus ($x = E_{h'}/E$). In particular, the four lowest moments provided by our fits,

$$Z_{hh'}(n, E) = \int_0^1 dx x^n f_{hh'}(x, E), \quad (1)$$

match the ones derived from 5×10^4 collisions simulated with EPOS-LHC (using the crmc package [18]) at different energies. In Fig.1–left we show for illustration the yields of light mesons in proton–air collisions at 10^6 GeV. Notice that the zero moment of $f_{hh'}(x, E)$ corresponds to the total number of particles h' created per collision, whereas the first moment is the fraction of energy taken by these particles. In the example, the average collision produces 52.9 charged pions and 7.9 kaons that take respectively 34.6% and 7.1% of the proton energy. Using SIBYLL 2.3C [19] we obtain

[‡]The details about these fits will be presented elsewhere.

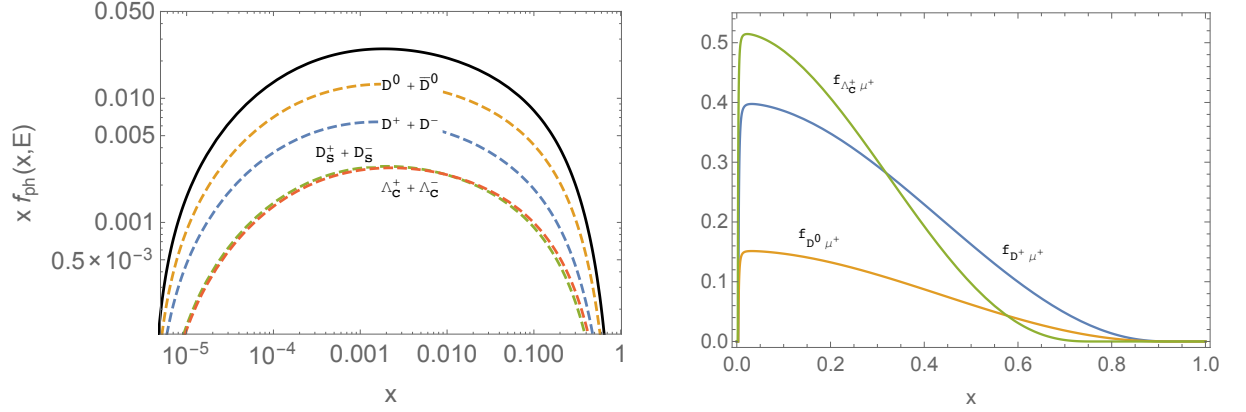


Figure 2: Left: Charmed-hadron yields in proton-air collisions at 10^6 GeV obtained with SIBYLL 2.3C [19]. Right: Muon yields in charmed hadron decays.

similar results: 51.6 charged pions and 8.5 kaons carrying 30.7% and 7.6% of the proton energy, respectively. The yields in pion and kaon collisions are analogous.

The decay of these light mesons will produce muons [20]. In Fig. 1–right we have included the decay yields $f_{h\mu}(x, E)$ in the ultrarelativistic limit, with the zero moment giving the branching ratio into muons in these decays.

(ii) *Muons from charmed-hadron decays.*

SIBYLL 2.3C has included charmed-hadron production: in Fig. 2 we plot for illustration the yields in proton collisions at 10^6 GeV. It is remarkable that these yields incorporate at least a fraction of the so called *forward* charm [21–23]. This refers to charm produced through a matrix element at any order that combines with a (spectator) valence quark of the projectile (*i.e.*, coalescence in the fragmentation region) or charm produced in diffractive collisions (after pomeron exchange the diffractive mass of the projectile is large enough to give a couple of charmed hadrons). In both cases the collision results into a forward charmed hadron carrying a large fraction x of the collision energy. Notice that perturbative calculations [24] combine amplitudes with fragmentation functions that (according to factorization theorems) do not depend on the initial state, whereas these codes use a fragmentation model that allows coalescence.

Once produced the D mesons and Λ_c baryons may decay giving muons (see the decay yields in Fig. 2 [8]). However, at $E \geq 10^6$ GeV they may also collide losing part of their energy. The inelasticity $K = 1 - \langle x \rangle$ in charmed hadron collisions with air is smaller than in pion or proton collisions. In [25, 26] $\langle x \rangle$ is estimated with PYTHIA [27] simulating light hadron collisions and then replacing (after the collision but before fragmentation) the leading up quark by a charm quark. The results for the fraction of energy carried by the leading charmed hadron after the collision can be approximated by a gaussian distribution with $\langle x \rangle = 0.56$, versus just $\langle x \rangle = 0.26$ for the leading pion in a 10^6 GeV pion collision.

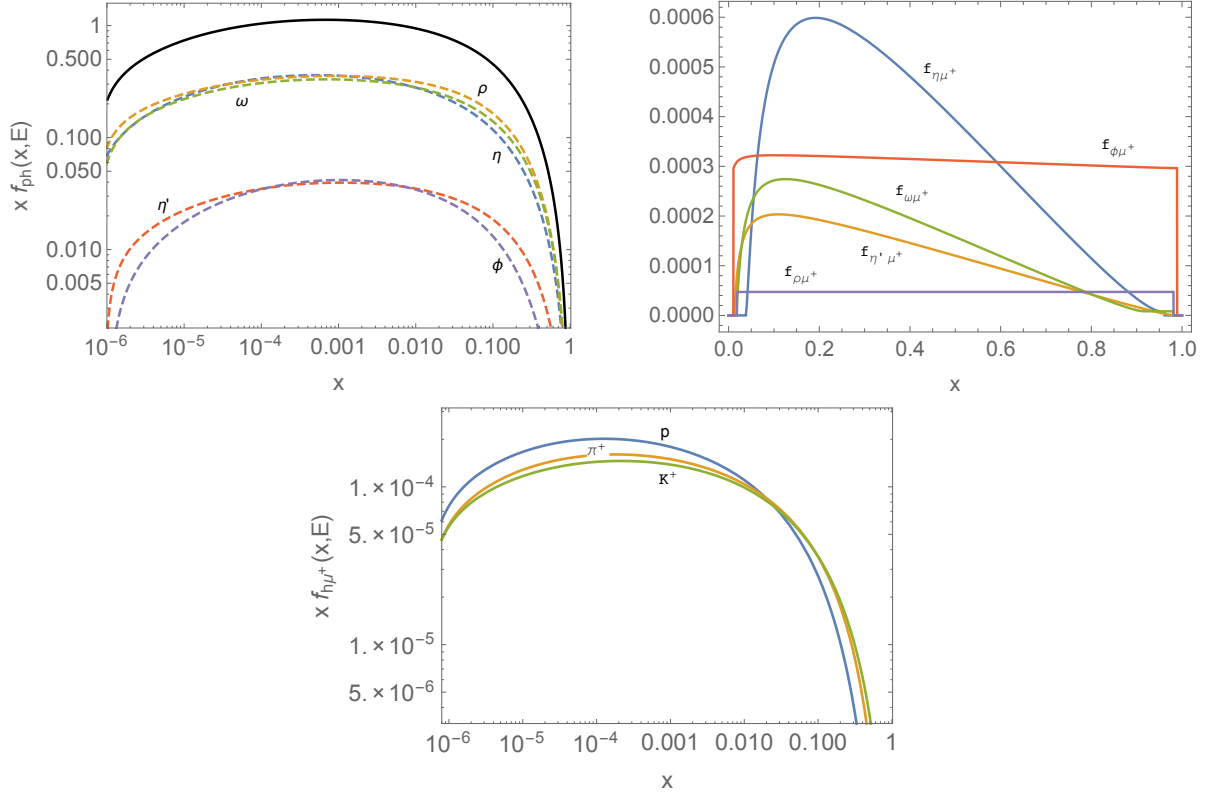


Figure 3: Unflavored meson yield in proton-air collisions at 10^6 GeV obtained with EPOS-LHC (left), muon yield in their decays (right), and muon yield through unflavored mesons in proton, pion and kaon collisions with air at 10^6 GeV (lower).

(iii) *Muons from the rare decays of unflavored mesons.*

The unflavored mesons η , ρ , ω , η' and ϕ , with masses between 0.5 and 1 GeV, include decay channels with muon pairs. For example, $\text{BR}(\eta \rightarrow \mu^+ \mu^- \gamma) = 3.1 \times 10^{-4}$ or $\text{BR}(\phi \rightarrow \mu^+ \mu^-) = 2.9 \times 10^{-4}$ [28]. These decay modes are more rare than in D -meson decays (*e.g.*, $\text{BR}(D^+ \rightarrow \bar{K}^0 \mu^+ \nu_\mu) = 0.092$), but this is partially compensated by the smaller mass and then the larger frequency of unflavored mesons in hadronic collisions. Moreover, they always decay promptly, whereas most D mesons and Λ_c baryons of $E > 10^7$ GeV collide in the air and lose energy instead of decaying.

In Fig. 3 we plot the yields of unflavored mesons in proton-air collisions at 10^6 GeV together with their decay yields into muons [8]. Since they decay almost instantly, we can obtain the muon yield in hadron collisions through unflavored mesons as

$$f_{h\mu}(x, E) = \int_x^1 dx' \frac{1}{x'} \sum_{h'=\eta, \rho, \dots} f_{hh'}(x', E/x) f_{h'\mu}(x/x'). \quad (2)$$

We include for illustration also in Fig. 3 the muon yield in proton, pion and kaon collisions with air at 10^6 GeV.

(iv) *Photon conversion into a muon pair.*

High energy photons appear in hadron collisions mostly through π^0 and η decays. We obtain with EPOS-LHC that photons take 20.6% of the energy in proton-air collisions at 10^6 GeV, and that this percentage is even larger in pion and kaon collisions (24.4% and 24.1%, respectively). The gamma conversion length into e^+e^- pairs is then

$$\frac{1}{\lambda_{\gamma}^{ee}(E, \rho)} = \frac{7/9 - b/3}{X_0} S_{\gamma}^{\text{tot}}(E, \rho) \quad (3)$$

where $S_{\gamma}^{\text{tot}}(E, \rho)$ is the LPM suppression [29, 30] (see next section), $X_0 = 37.1$ g/cm² and (in air) $b = 0.012$. The conversion into muon pairs will appear suppressed by a factor of m_e^2/m_{μ}^2 , $\lambda_{\gamma}^{\mu\mu} \approx 2 \times 10^6$ g/cm², and the fraction of energy going to each muon is distributed [31]

$$f_{\gamma\mu^+}(x, E) = \frac{\lambda_{\gamma}^{\text{int}}(E, \rho)}{X_0} \left(\frac{m_e}{m_{\mu}}\right)^2 \left(\frac{2}{3} - \frac{b}{2} + \left(\frac{4}{3} + 2b\right) \left(x - \frac{1}{2}\right)^2\right). \quad (4)$$

This is then a very rare process ($m_e^2/m_{\mu}^2 = 2.4 \times 10^{-5}$) but one where all the photon energy goes into muons. Notice also that the LPM effect will favor the conversion into muons (relative to electrons) at energies above

$$E_{\text{LPM}} \approx 7.7 \frac{X_0}{\rho} \text{ TeV/cm}. \quad (5)$$

(v) *Photon conversion into a vector meson decaying into muons.*

In the previous process the photon fluctuates into a virtual muon pair that goes on shell after an EM interaction with an air nucleus. However, the photon may also fluctuate into a $q\bar{q}$ pair, *i.e.*, a virtual vector meson that becomes real after a hadronic (pomeron mediated) interaction with the nucleus. This fluctuation is less likely due to the larger mass of the meson, but the suppression is partially compensated by the larger coupling in the hadronic process.

It turns out that in 1 out of 400 collisions (and even more often at low energies near a hadronic resonance) the photon behaves like a rho meson. The most frequent photonuclear collision is then an inelastic process resulting into a multiplicity of pions, but over 10% of them are exclusive ($\gamma p \rightarrow \rho p$) or dissociative ($\gamma p \rightarrow \rho X$) conversions where the ρ meson gets almost all of the photon energy. We will also consider the γ conversion into a J/ψ meson (a $c\bar{c}$ state), more rare than the ρ (specially at lower energies) but with a much larger branching ratio into $\mu^+\mu^-$ (around a 5.9%).

In our estimate for these processes we have extrapolated the HERA observations at $\sqrt{s} < 300$ GeV [32, 33] up to $\sqrt{s} < 300$ TeV using a two-pomeron scheme:

$$\begin{aligned} \sigma_{\text{tot}}(\gamma p) &= 69.0 s^{0.08} + 175 s^{-0.60}, \\ \sigma(\gamma p \rightarrow \rho p) &= 4.9 s^{0.11} + 21 s^{-0.40}, \\ \sigma(\gamma p \rightarrow J/\psi p) &= 0.0016 s^{0.41}, \end{aligned} \quad (6)$$

where s is given in GeV² and the cross sections in μb . To include dissociative conversions [34, 35] we have just added a 60% to the exclusive cross sections above, and we have assumed that the scaling to go from a proton to a nucleus target coincides with the one in pion collisions.

3 Cascade equations and muon flux

We will solve numerically the (longitudinal) cascade equations for 15 hadron species h ($p, n, \bar{p}, \bar{n}, \pi^\pm, K^\pm, K_L, D^\pm, D^0, \bar{D}^0, D_s^\pm, \Lambda_c^\pm$), photons, electrons and muons, with μ^\pm from the prompt decay of unflavored mesons included in the yields $f_{h\mu}(x, E)$ and $f_{\gamma\mu}(x, E)$ (see previous section). The initial flux ($t = 0$) will correspond to a single primary of energy E_0 , whereas the secondary fluxes will be defined for $E \leq E_0$. The generic equations are [20]

$$\begin{aligned} \frac{d\Phi_i(E, t)}{dt} = & -\frac{\Phi_i(E, t)}{\lambda_i^{\text{int}}(E)} - \frac{\Phi_i(E, t)}{\lambda_i^{\text{dec}}(E, t)} + \sum_{j=h, \gamma, e} \int_{E/E_0}^1 dx \frac{f_{ji}(x, E/x)}{x} \frac{\Phi_j(E/x, t)}{\lambda_j^{\text{int}}(E/x)} + \\ & \sum_{k=h} \int_{E/E_0}^1 dx \frac{f_{ki}^{\text{dec}}(x, E/x)}{x} \frac{\Phi_k(E/x, t)}{\lambda_j^{\text{dec}}(E/x, t)}, \end{aligned} \quad (7)$$

where $\Phi_i = dN_i/dE$, t is the slant depth and the interaction/decay lengths are expressed in g/cm^2 . We will focus on particles with energy between 1 TeV and the energy of the primary.

The EM component of the shower will be started in hadronic collisions through the decay of neutral mesons and other hadronic resonances (we obtain $f_{h\gamma}(x, E)$ from a fit to EPOS-LHC simulations); we neglect the production of electrons in hadron and muon decays and also the photonuclear collisions of electrons. The cascade equations for photons and electrons read then [1]

$$\begin{aligned} \frac{d\Phi_\gamma(E, t)}{dt} = & -\frac{\Phi_\gamma(E, t)}{\lambda_\gamma^{\text{int}}(E, t)} + \sum_{j=h} \int_{E/E_0}^1 dx \frac{f_{j\gamma}(x, E/x)}{x} \frac{\Phi_j(E/x, t)}{\lambda_j^{\text{int}}(E/x)} \\ & + \int_{E/E_0}^1 dx \frac{f_{e\gamma}(x, E/x, t)}{x} \frac{\Phi_e(E/x, t)}{\lambda_e^{\text{int}}(E/x, t)}, \end{aligned} \quad (8)$$

and

$$\begin{aligned} \frac{d\Phi_e(E, t)}{dt} = & -\frac{\Phi_e(E, t)}{\lambda_e^{\text{int}}(E, t)} + \int_{E/E_0}^1 dx \frac{2f_{\gamma e}(x, E/x, t)}{x} \frac{\Phi_\gamma(E/x, t)}{\lambda_\gamma^{\text{int}}(E/x, t)} \\ & + \int_{E/E_0}^{1-x_{\min}} dx \frac{f_{e\gamma}(1-x, E/x, t)}{x} \frac{\Phi_e(E/x, t)}{\lambda_e^{\text{int}}(E/x, t)}, \end{aligned} \quad (9)$$

where $x_{\min}(E) = E_{\min}^\gamma/E$ and we have used that $f_{ee}(x, E) = f_{e\gamma}(1-x, E)$. The interaction lengths are

$$\begin{aligned} \frac{1}{\lambda_\gamma^{\text{int}}(E, t)} &= \frac{7-3b}{9X_0} \left(S_\gamma^{\text{tot}}(E, \rho) + \frac{m_e^2}{m_\mu^2} \right) + \frac{\sigma_{\gamma A}^{\text{had}}}{m_A}; \\ \frac{1}{\lambda_e^{\text{int}}(E, t)} &= \frac{\int_{x_{\min}}^1 dx \phi(x)}{X_0} S_e^{\text{tot}}(E, \rho), \end{aligned} \quad (10)$$

with m_A the target mass (in grams) in an average hadronic collisions in the air (*i.e.*, $A = 14.6$), while the EM yields are [31]

$$\begin{aligned} f_{\gamma e}(x, E, t) &= \frac{\lambda_\gamma^{\text{int}}(E, t)}{X_0} S_\gamma(x, E, \rho) \psi(x); & \psi(x) &= \frac{2}{3} - \frac{b}{2} + \left(\frac{4}{3} + 2b \right) \left(x - \frac{1}{2} \right)^2, \\ f_{e\gamma}(x, E, t) &= \frac{\lambda_e^{\text{int}}(E, t)}{X_0} S_e(x, E, \rho) \phi(x); & \phi(x) &= x + \frac{1-x}{x} \left(\frac{4}{3} + 2b \right). \end{aligned} \quad (11)$$

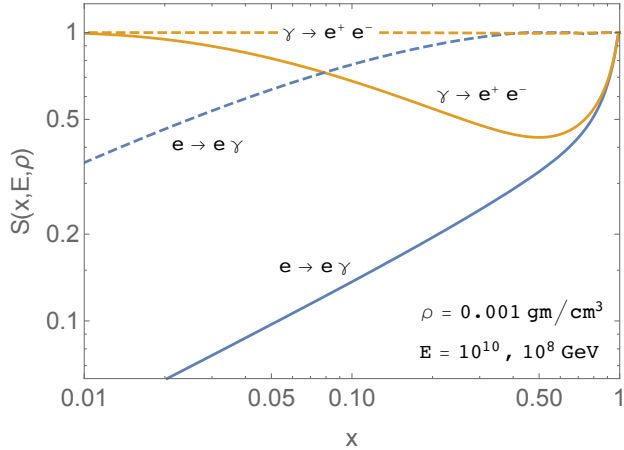


Figure 4: LPM reduction in $d\sigma(e \rightarrow e\gamma)/dx$ and $d\sigma(\gamma \rightarrow e^+e^-)/dx$ in air at $\rho = 0.001 \text{ g/cm}^3$ for $E = 10^{10} \text{ GeV}$ (solid), 10^8 GeV (dashes), with x the fraction of energy carried by the final γ and e^- , respectively. We have used the (non-recursive) expressions in [29].

The factors $S_{\gamma,e}^{\text{tot}}$ and $S_{\gamma,e}$ above express the LPM reduction in the total and the differential cross sections for $\gamma \rightarrow e^+e^-$ and $e \rightarrow e\gamma$ in the air. In Fig. 4 we plot $S_{\gamma,e}(x, E, \rho)$ for $E = 10^8, 10^{10} \text{ GeV}$ and $\rho = 0.001 \text{ g/cm}^3$; the suppression in the total cross section is in those cases $S_e^{\text{tot}} = 0.043$ and $S_\gamma^{\text{tot}} = 0.58$ at 10^{10} GeV but just $S_e^{\text{tot}} = 0.33$ and $S_\gamma^{\text{tot}} = 0.99$ at 10^8 GeV .

We obtain the nuclear cross sections needed in the hadronic interaction lengths ($\lambda_h^{\text{int}} = m_A/\sigma_{hA}$) with EPOS-LHC, and we use isospin symmetry to deduce the whole set of yields from the ones in p , π^+ and K^+ collisions. The charmed hadron yields have been deduced with SIBYLL2.3C (we have normalized the EPOS-LHC yields of light mesons and baryons to subtract the energy taken by these D mesons and Λ_c baryons). As for the muons, we neglect energy loss as they propagate, but in the next section we will calculate the probability for a catastrophic energy deposition in the air near the surface. For the atmosphere we assume [36] (in g/cm^3)

$$\rho(h) = \begin{cases} 1.210 \times 10^{-10} (44.33 - h)^{4.253}, & h < 11 \text{ km}; \\ 2.053 \times 10^{-3} \exp\left(-\frac{h}{6.344 \text{ km}}\right), & h > 11 \text{ km}. \end{cases} \quad (12)$$

We have taken 200 logarithmic bins of energy with $E_{\text{min}} = 10 \text{ TeV}$ and 2500 linear bins of altitude with $h_0 = 70 \text{ km}$, and we have checked that the transport through the atmosphere conserves the total energy in the shower. Our results are summarized in Fig. 5. There we plot the particle flux (number of particles per unit energy) at the ground level for several primaries, all of them with $E = 10^{10.5} \text{ GeV}$.

The upper figures include a proton from zenith angles $\theta_z = 60^\circ$ (left) and $\theta_z = 0^\circ$ (right). We find a total of 0.0065 muons with $E \geq 10^8 \text{ GeV}$ in the first case and 0.0052 muons in a vertical shower. This implies, respectively, that around 1 in 150 or 1 in 190 showers include such a muon.

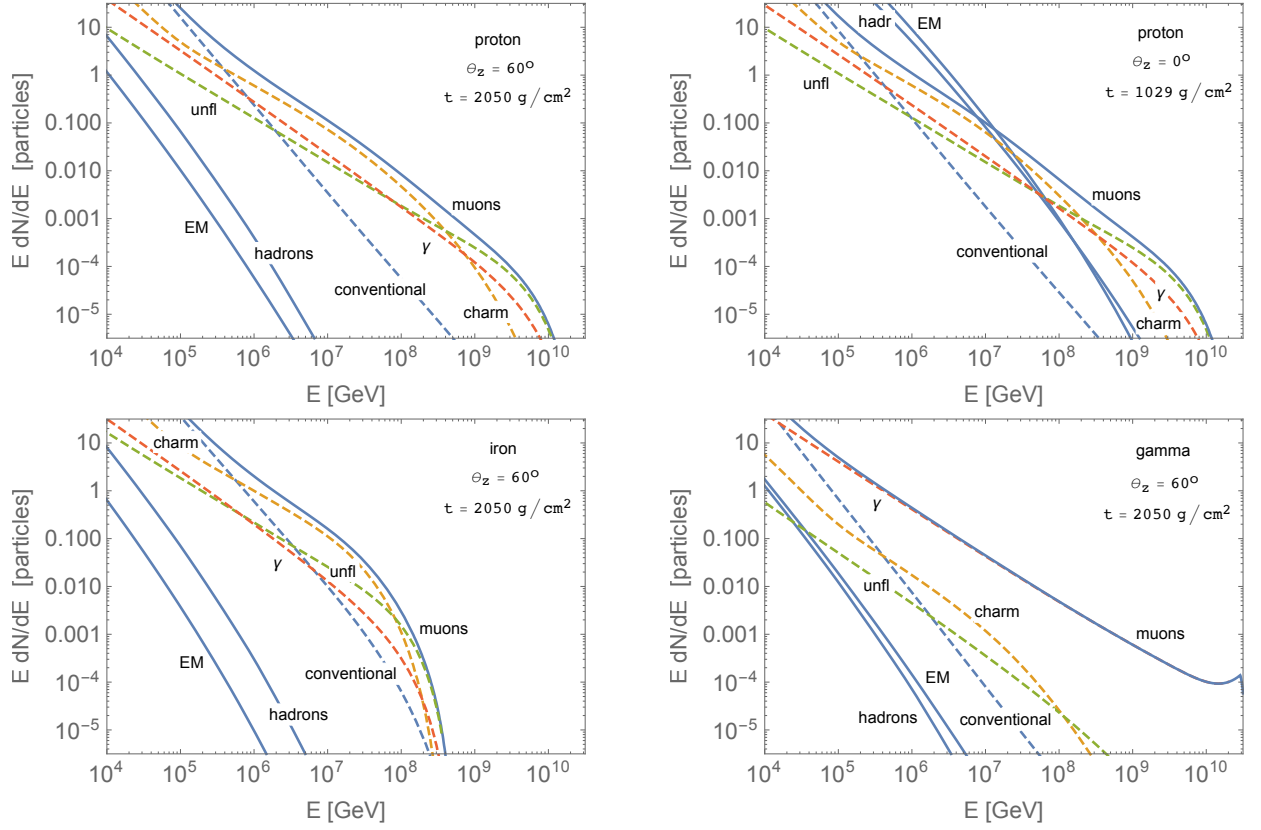


Figure 5: Particle count at the ground level for a $10^{10.5}$ GeV proton (top left), iron nucleus (bottom left) or gamma ray (bottom right) coming from $\theta_z = 60^\circ$, and for a vertical proton of the same energy (top right). The EM line includes photons and electrons, and the dashed lines indicate the different contributions to the muon flux (the γ line includes the muons from $\gamma \rightarrow \mu\mu$ and from $\gamma \rightarrow \rho, J/\psi \rightarrow \mu\mu$).

The contribution to this muon count from unflavored mesons and gamma conversions is basically independent from the shower inclination, while the charm contribution has a 40% reduction for vertical showers (it goes from 0.0030 to 0.0018). In the inclined proton shower charm decays generate 46% of the $E > 10^8$ GeV muons, unflavored decays 30% and photon conversions 23%, being the contribution from $\gamma \rightarrow \mu^+\mu^-$ three times larger than the one from $\gamma \rightarrow J/\psi \rightarrow \mu^+\mu^-$.

In the lower figures we plot the fluxes for iron (left) or photon (right) showers of also $E = 10^{10.5}$ GeV, both from a zenith inclination $\theta_z = 60^\circ$. The number of muons with energy $E > 10^8$ GeV is, respectively, 0.0010 and 0.0053. This means that only 1 in 1000 iron showers or 1 in 186 photon showers include such a muon. In an iron primary charm decays contribute a 28% to this muon count, whereas in gamma showers 99% of the muons come from gamma conversions (71% in EM interactions and 28% through J/ψ decays). We also see that the conventional contribution from pion and kaon decays is negligible both for proton or gamma primaries, but it is more significant (2.1%) in iron showers. We find remarkable that in photon showers the conversions $\gamma \rightarrow \mu^+\mu^-$ and

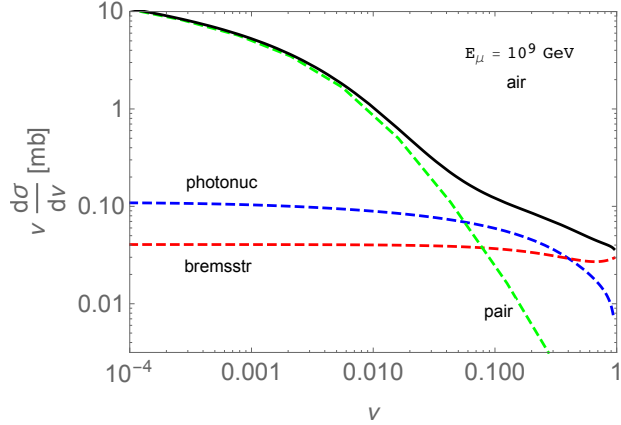


Figure 6: Cross section to deposit a fraction ν of energy in muon collisions in the air.

$\gamma \rightarrow J/\psi \rightarrow \mu^+\mu^-$ give many more muons than pion and kaon decays even at lower energies (see the discussion on muons from inelastic photonuclear collisions in [37]). We notice as well that the LPM effect on the muon count is negligible in iron or proton showers, while in the average $10^{10.5}$ GeV photon shower it increases the number of these very high energy muons in just a 2%.

4 Muon energy depositions near the surface

High-energy muons may radiate a significant fraction of their energy through three different processes: bremsstrahlung, pair production or photonuclear interactions [38]. The first two processes would start an EM shower, whereas photonuclear collisions would define a hadronic sub-shower. In inclined events these energy depositions could occur very deep in the atmosphere, when most of the shower energy has been absorbed. In Fig. 6 we plot the differential cross section for these radiative processes, being ν the fraction of the muon energy deposited in the air.

The probability that a muon of energy E has an interaction within a depth $\Delta X = 500 \text{ g/cm}^2$ where it radiates a minimum energy E_0 is

$$p(E_0, E) = \frac{\Delta X}{m_A} \int_{E_0/E}^1 d\nu \frac{d\sigma}{d\nu}, \quad (13)$$

with values larger than 1 expressing the average number of depositions. For an incident flux $\Phi_\mu(E)$ the probability to have the same type of energy deposition is then

$$p(E_0) = \frac{\Delta X}{m_A} \int_{E_0}^{\infty} dE \Phi_\mu(E) \int_{E_0/E}^1 d\nu \frac{d\sigma}{d\nu}. \quad (14)$$

Our results for the 3 primaries considered in the previous section are the following. In a $10^{10.5}$ GeV proton shower from $\theta_z = 60^\circ$ the probability to have an energy deposition above 10^6 GeV is 0.17, *i.e.*, we can expect such an anomaly in one out of 6 proton showers. $E \geq 10^7$ depositions would

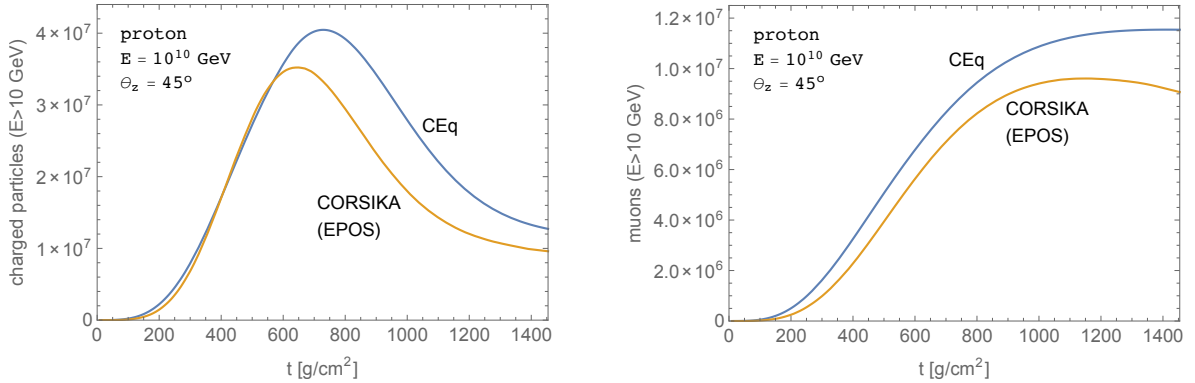


Figure 7: Number of charged particles (left) or muons (right) with $E > 10$ GeV in a 10^{10} GeV proton shower at different slant depths obtained with cascade equations and CORSIKA.

be much less frequent: around in 1 out of 330 showers. In contrast, the $E \geq 10^6$ GeV depositions would occur in only 1 out of 92 iron showers, and the deposition would be above 10^7 GeV in one per 7000 iron showers. For a photon primary the spectrum of high-energy muons is much harder than in hadron showers (see Fig. 4). Since a 10^9 – 10^{10} GeV muon loses around 0.4% of its energy per 1000 g/cm² of air, *most* muons in this energy range (appearing in around 1 in 200 photon showers) will start $O(10^7$ GeV) EM mini-showers near the ground.

5 Cascade equations versus Monte Carlo simulations

We would like to briefly address some of the limitations and the validity of the method that we have used for the study of EASs. Our simplified cascade equations are a fast and flexible way to estimate the relative relevance of a given effect, but they can not substitute the more precise results obtained with Monte Carlo codes like AIRES [16] and CORSIKA [39] or with hybrid models (combining Monte Carlo methods with cascade equations) like CONEX [40] and SENECA [41]. Our method seems specially useful to estimate the relative effect of a rare process (*e.g.*, photon conversions into muon pairs) whose accurate study with simulations would require a very large statistics.

We have used 1-dimensional cascade equations that neglect the lateral versus the longitudinal development of the shower. As a consequence, we obtain a poorer approximation at lower energies, where the transverse momentum of the particles may be relatively important and imply a larger lateral displacement. In addition, to simplify the equations we have not included effects, like energy loss by ionization, that are also important at low energies. The energy binning, the finite value of the depth intervals or the simple model that we have used for the atmosphere are sources of uncertainty as well.

To calibrate the accuracy of our results we have solved the cascade equations for a 10^{10} GeV proton shower from $\theta_z = 45^\circ$ and have extended the range of energies down to 10 GeV. We have

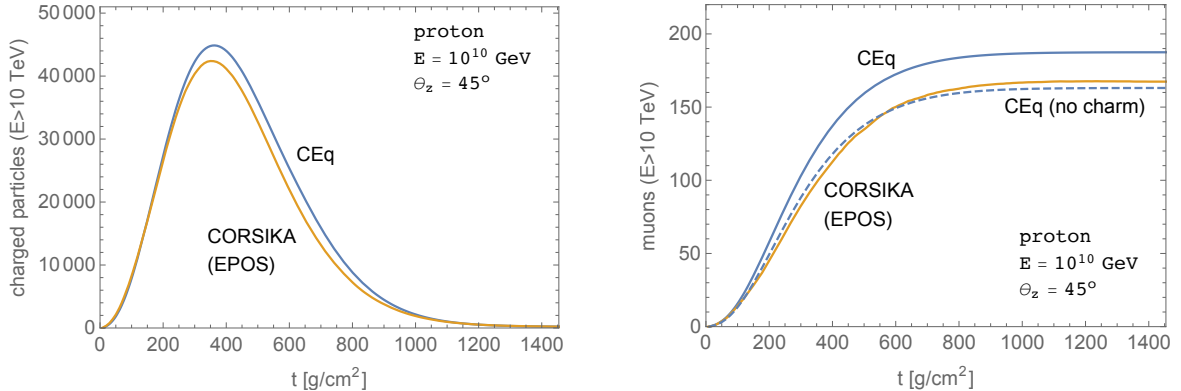


Figure 8: Number of charged particles (left) or muons (right) with $E > 10$ TeV in a 10^{10} GeV proton shower at different slant depths obtained with cascade equations and CORSIKA. In dashes, we have subtracted the muons from charm decays.

then averaged 30 showers simulated with CORSIKA (running with the EPOS-LHC option and a 10^{-6} thinning) with the same primary and minimum energy. In Fig. 7 we plot the total number of charged particles (including muons) with $E > 10$ GeV at different atmospheric depths (left), together with the evolution in the number of muons (right). The Monte Carlo simulations imply a value of X_{max} and a number of particles 20% smaller than the one obtained with cascade equations.

The analysis that we have presented in the previous sections, however, involves muons of much higher energy, where we expect more accuracy. To confirm that we have run 30 more proton showers but taking a larger value of the minimum energy: $E > 10$ TeV. The comparison with the results from the cascade equations, in Fig. 8, show now a much better agreement. We obtain that the differences in X_{max} and in number of charged particles are within a 5%. The difference is more significant in the number of muons with $E > 10$ TeV, but this is due to the absence of charm in the CORSIKA simulation with the EPOS-LHC option; once we subtract the muons from charm (yields deduced with SIBYLL 2.3C) we obtain the almost perfect agreement shown in Fig. 8-right.

6 Summary and discussion

In studies of EASs the connection between the primary CR and the secondary particles observable at the surface usually relies on a Monte Carlo simulation. It is then necessary to make sure that all the relevant effects are included, and 1-dimensional cascade equations may be a useful tool. We find that to account for the most energetic muons in a shower one has to include, in addition to charmed hadrons, the rare decays of unflavored mesons and the photon conversions into muon pairs and J/ψ mesons. This is clear in photon showers at all muon energies (the conversions produce more muons than pion and kaon decays even at 10^4 GeV, see Fig. 5), but also in proton showers at $E \geq 10^9$ GeV. Remarkably, the EAS simulator CORSIKA [39] with the SIBYLL 2.3C option would

include all of the processes discussed here except for the quasielastic conversion of a photon into a J/ψ meson. Notice, however, that for proton or iron primaries this contribution is subleading: photon conversions account for 23% of all muons of $E > 10^8$ GeV in the shower, and only 24% of those muons come from J/ψ decays. Although all the muon sources are then standard and known, we think that the complete analysis of their (energy dependent) relative weight can not be found in previous literature.

The fluctuations in the value of X_{\max} in EASs are caused by the details (interaction point, multiplicity, inelasticity) in the first hadronic collisions high in the atmosphere. Once the shower has reached X_{\max} , its hadron and EM components include millions of particles sharing most of the shower energy, and the individual fluctuations appear then *averaged*. Hadrons or electrons are unable to produce large fluctuations in any observable after X_{\max} because all of them have an energy much smaller than the total shower energy at that depth. What we discuss here is arguably the only possible source of fluctuations in the longitudinal development of an EAS *after* X_{\max} : very high energy muons with catastrophic depositions near the surface. Only muons can take a large amount of energy and deposit it near the ground in an inclined shower. This effect would make possible that two inclined showers with the same primary and the same value of X_{\max} evolve different as they get to the ground. Our analysis here intends to quantify the frequency of such events, and it may motivate a more complete study (using Monte Carlo or hybrid models) of its possible relevance at current or future EAS observatories.

Our analysis is based on a numerical solution to the longitudinal cascade equations through the atmosphere. At high energies the method is able to incorporate easily and precisely each one of the new effects (Monte Carlo methods may be less efficient to capture the rare effects discussed here). Our results are consistent with the ones in [10], that focus on the total (inclusive) atmospheric muon flux and emphasize the relevance of unflavored meson decays, although photon conversions into muon pairs and J/ψ mesons are not included there.

We estimate that 1 in 43 inclined events started by a $10^{10.5}$ GeV proton primary contains a muon taking more than 0.1% of the total shower energy (*i.e.*, $E > 10^{7.5}$ GeV), that 1 in 6 proton showers include a radiative energy deposition above 10^6 GeV within 500 g/cm^2 near the surface, and that in 1 in 330 showers this deposition is above 10^7 GeV. These frequencies are different for iron or gamma primaries (only 1 in 60 iron showers or 61 photon showers includes such a muon). The appearance of an EM shower after most of the parent EAS has been absorbed (*i.e.*, beyond 1500 g/cm^2) could introduce rare fluctuations in the muon to electron count at the ground level [15], something that may be measured with enough accuracy after the upgrade in the surface detectors at AUGER [42]. Since no hadrons can keep 10^6 – 10^7 GeV after such depth, the fluctuations may provide an indirect signal of the hadronic processes discussed here. In particular, they may be an interesting channel to search for (the so far elusive) atmospheric charm. These very energetic muons are also of interest at ν telescopes, where a determination of the $E \geq 100$ TeV muon flux and its correlation with the neutrino flux at the same energies could also reveal a contribution from

atmospheric charm.

Hadronic simulators like EPOS-LHC or SIBYLL give predictions at extreme energies, well beyond the ones achieved at particle colliders. The muons discussed here are a probe of those energies. We think that this could make them useful in the study of both the hadronic cross sections in this regime and the composition of the highest energy CRs.

Acknowledgments

The authors would like to thank T. Pierog and R. Ulrich for providing the *Cosmic Ray Monte Carlo* package [18]. This work has been supported by MICINN of Spain (FPA2016-78220, RED2018-102661-T) and by Junta de Andalucía (SOMM17/6104/UGR and FQM101). CG and JSM acknowledge a grant from *Programa Operativo de Empleo Juvenil* (Junta de Andalucía) and MG an *Iniciación a la Investigación* fellowship from the University of Granada.

References

- [1] T. K. Gaisser, “Cosmic rays and particle physics,” Cambridge, UK: Univ. Pr. (1990) 279 p.
- [2] M. Albrow, PoS EDSU **2018** (2018) 048 doi:10.22323/1.335.0048 [arXiv:1811.02047 [physics.ins-det]].
- [3] S. Baur, H. Dembinski, T. Pierog, R. Ulrich and K. Werner, arXiv:1902.09265 [hep-ph].
- [4] A. Aab *et al.* [Pierre Auger Collaboration], Phys. Rev. D **91** (2015) no.3, 032003 Erratum: [Phys. Rev. D **91** (2015) no.5, 059901].
- [5] P. Gondolo, G. Ingelman and M. Thunman, Astropart. Phys. **5** (1996) 309.
- [6] R. Enberg, M. H. Reno and I. Sarcevic, Phys. Rev. D **78** (2008) 043005.
- [7] J. I. Illana, M. Masip and D. Meloni, JCAP **0909** (2009) 008.
- [8] J. I. Illana, P. Lipari, M. Masip and D. Meloni, Astropart. Phys. **34** (2011) 663.
- [9] T. Pierog, I. Karpenko, J. M. Katzy, E. Yatsenko and K. Werner, Phys. Rev. C **92** (2015) 034906.
- [10] A. Fedynitch, F. Riehn, R. Engel, T. K. Gaisser and T. Stanev, “The hadronic interaction model Sibyll-2.3c and inclusive lepton fluxes,” arXiv:1806.04140 [hep-ph].
- [11] F. Tenholt *et al.* [IceCube Collaboration], “The IceCube Neutrino Observatory - Contributions to ICRC 2017 Part III: Cosmic Rays,” arXiv:1710.01194 [astro-ph.HE].

- [12] A. G. Bogdanov, R. P. Kokoulin, G. Mannocchi, A. A. Petrukhin, O. Saavedra, V. V. Shutenko, G. Trincherro and I. I. Yashin, *Astropart. Phys.* **98** (2018) 13.
- [13] A. A. Kochanov, A. D. Morozova, T. S. Sinegovskaya and S. I. Sinegovsky, *J. Phys. Conf. Ser.* **1181** (2019) no.1, 012054.
- [14] O. Tascau, R. Engel, K. H. Kampert and M. Risse, “Investigation of backgrounds for horizontal neutrino showers at ultra-high energy,” proceedings of the 30th ICRC (2007), pag. 133, FZKA-7340ZH.
- [15] C. A. García Canal, J. I. Illana, M. Masip and S. J. Sciutto, *Astropart. Phys.* **85** (2016) 50.
- [16] S. J. Sciutto, *AIRES, a system for air shower simulation and analysis*. See www2.fisica.unlp.edu.ar/aires
- [17] A. Aab *et al.* [Pierre Auger Collaboration], “The Pierre Auger Observatory Upgrade - Preliminary Design Report,” arXiv:1604.03637 [astro-ph.IM]. FERMILAB-DESIGN-2016-05
- [18] <https://web.iikp.kit.edu/rulrich/crmc.html>
- [19] E. J. Ahn, R. Engel, T. K. Gaisser, P. Lipari and T. Stanev, *Phys. Rev. D* **80** (2009) 094003.
- [20] P. Lipari, *Astropart. Phys.* **1** (1993) 195.
- [21] S. J. Brodsky, P. Hoyer, C. Peterson and N. Sakai, *Phys. Lett.* **93B** (1980) 451.
- [22] F. Halzen and L. Wille, *Phys. Rev. D* **94** (2016) no.1, 014014.
- [23] F. Carvalho, A. V. Giannini, V. P. Goncalves and F. S. Navarra, *Phys. Rev. D* **96** (2017) no.9, 094002.
- [24] R. Gauld, J. Rojo, L. Rottoli, S. Sarkar and J. Talbert, *JHEP* **1602** (2016) 130.
- [25] R. Barcelo, J. I. Illana, M. D. Jenkins and M. Masip, *Phys. Rev. D* **83** (2011) 034027.
- [26] A. Bueno, A. Gascon, J. I. Illana and M. Masip, *JCAP* **1202** (2012) 028.
- [27] T. Sjostrand, S. Mrenna and P. Z. Skands, *JHEP* **0605** (2006) 026.
- [28] M. Tanabashi *et al.* [Particle Data Group], *Phys. Rev. D* **98** (2018) no.3, 030001.
- [29] T. Stanev, C. Vankov, R. E. Streitmatter, R. W. Ellsworth and T. Bowen, *Phys. Rev. D* **25** (1982) 1291.
- [30] L. Gerhardt and S. R. Klein, *Phys. Rev. D* **82**, 074017 (2010).
- [31] B. Rossi and K. Greisen, *Rev. Mod. Phys.* **13** (1941) 240.

- [32] P. Merkel, “Diffractive photoproduction of heavy vector mesons at HERA,” DESY-THESIS-1999-030.
- [33] A. Aktas *et al.* [H1 Collaboration], Eur. Phys. J. C **46** (2006) 585.
- [34] S. Chekanov *et al.* [ZEUS Collaboration], Eur. Phys. J. C **26** (2003) 389.
- [35] D. Bendova, J. Cepila and J. G. Contreras, Phys. Rev. D **99** (2019) no.3, 034025.
- [36] K. Maeda, Fortsch. Phys. **21** (1973) 113.
- [37] F. Cornet, C. A. Garcia Canal, A. Grau, G. Pancheri and S. J. Sciutto, Phys. Rev. D **92** (2015) 114011.
- [38] D. E. Groom, N. V. Mokhov and S. I. Striganov, Atom. Data Nucl. Data Tabl. **78** (2001) 183.
- [39] D. Heck, J. Knapp, J. N. Capdevielle, G. Schatz and T. Thouw, *CORSIKA: A Monte Carlo code to simulate extensive air showers*, FZKA-6019. See reports FZKA 7525 and KIT-SWP-6 in <https://web.iip.kit.edu/heck/publications/> for the photon conversions into muon pairs and rho mesons, respectively.
- [40] T. Bergmann, R. Engel, D. Heck, N. N. Kalmykov, S. Ostapchenko, T. Pierog, T. Thouw and K. Werner, Astropart. Phys. **26** (2007) 420.
- [41] H. J. Drescher and G. R. Farrar, Phys. Rev. D **67** (2003) 116001.
- [42] A. Aab *et al.* [Pierre Auger Collaboration], Nucl. Instrum. Meth. A **798** (2015) 172.